LETTER

doi:10.1038/nature12763

Face-to-face transfer of wafer-scale graphene films

Libo Gao[1,2], Guang-Xin Ni[1,3], Yanpeng Liu[2], Bo Liu[1,2], Antonio H. Castro Neto[1,3] & Kian Ping Loh[1,2]

Graphene has attracted worldwide interest since its experimental discovery[1,2], but the preparation of large-area, continuous graphene film on SiO_2/Si wafers, free from growth-related morphological defects or transfer-induced cracks and folds, remains a formidable challenge[3]. Growth of graphene by chemical vapour deposition on Cu foils[4–7] has emerged as a powerful technique owing to its compatibility with industrial-scale roll-to-roll technology[6]. However, the polycrystalline nature and microscopic roughness of Cu foils means that such roll-to-roll transferred films are not devoid of cracks and folds[6,7]. High-fidelity transfer or direct growth of high-quality graphene films on arbitrary substrates is needed to enable wide-ranging applications in photonics or electronics, which include devices such as optoelectronic modulators, transistors, on-chip biosensors and tunnelling barriers[3,8,9]. The direct growth of graphene film on an insulating substrate, such as a SiO_2/Si wafer, would be useful for this purpose, but current research efforts remain grounded at the proof-of-concept stage, where only discontinuous, nanometre-sized islands can be obtained[10]. Here we develop a face-to-face transfer method for wafer-scale graphene films that is so far the only known way to accomplish both the growth and transfer steps on one wafer. This spontaneous transfer method relies on nascent gas bubbles and capillary bridges between the graphene film and the underlying substrate during etching of the metal catalyst, which is analogous to the method used by tree frogs to remain attached to submerged leaves[11,12]. In contrast to the previous wet[4,5,13–15] or dry[6,7] transfer results, the face-to-face transfer does not have to be done by hand and is compatible with any size and shape of substrate; this approach also enjoys the benefit of a much reduced density of transfer defects compared with the conventional transfer method. Most importantly, the direct growth and spontaneous attachment of graphene on the underlying substrate is amenable to batch processing in a semiconductor production line, and thus will speed up the technological application of graphene.

Much effort has been directed to controlling the grain size[15,16], doping[17] and heterostructure[18] of graphene by fine-tuning growth conditions during chemical vapour deposition (CVD), but there has been a lack of breakthroughs in the after-growth transfer process of the graphene film[3]. Conventional transfer methods for CVD graphene can be classified as either dry[6,7] or wet[4,5,13–15] transfer, depending on the environment in which graphene touches the target substrate. The dry transfer method seems to be more applicable to industrial applications, because it can realize a 30-inch graphene film on a flexible substrate[6], but plenty of transfer defects occur—for example, cracks, folds and wrinkles[6,7]. The wet transfer method is generally difficult to scale up, and the surface tension experienced by the floating graphene at the air–water interface causes warping, rippling and rolling of the films during transfer.

The inspiration for our face-to-face method is found in the study of how the feet of a terrestrial beetle or tree frog remain attached to a fully submerged leaf[11,12]. Microscopic observations reveal that air bubbles that are trapped around the feet of the beetle form capillary bridges and keep the beetle's feet attached to the submerged leaf. In a similar fashion, the formation of capillary bridges, as indicated schematically in Fig. 1a, ensures that the graphene film remains attached to the substrate and does not undergo delamination during the etching process (Fig. 1b). During the etching of the copper film between the graphene and the SiO_2/Si substrate, dissolution of the copper generates voids and channels, and these create capillary forces that allow the liquid etchant to infiltrate between the graphene film and the substrate. In the case of hydrophobic graphene surfaces[19], the unfavourable interactions between the water molecules and the soft graphene film induce instability of the planar interface, which leads to fluctuations of the water interface and spontaneous cavitation. Strong negative pressure will operate in short capillary bridges, resulting in long-ranged attraction between the contacting surfaces. In fact, such capillary adhesion forces can be larger than the van der Waals interaction between the two solids. We suggest that the evolution of bubbles during the etching process contributes to the formation of capillary bridges between the graphene–substrate interfaces, thus allowing the graphene film to remain attached to the substrate even with the infiltration of liquid. However, gas bubbles can also generate buoyancy forces that will separate the graphene film from the underlying substrate, and this is in fact the situation exploited in the conventional float transfer process. Therefore, the fate of the graphene film—with regard to either delamination from, or adhesion to, the substrate—is decided by whether a sufficient number of capillary bridges can be formed between the graphene and the substrate to counteract the pull-off forces due to buoyancy.

The presence of gas bubbles under the graphene can be seen by atomic force microscopy (AFM) imaging of the surface after CVD growth. Inductively coupled plasma CVD (ICP-CVD), required for the growth of graphene (see Methods), produces energetic ions that can be absorbed by the metal catalyst at high temperature. As the temperature is reduced at the end of the growth process, some gas precipitates at the surface and gets trapped between the impermeable graphene[20] and the substrate, forming bubbles. These bubbles alter the adhesion and strain properties of graphene, which are manifested as bright spots in the AFM phase contrast images (Supplementary Fig. 2). To facilitate the formation of capillary bridges, a pre-treatment step involving plasma nitridation of the SiO_2/Si wafer is helpful. Our experiments showed that without this treatment step, the graphene film delaminates at the end of the etching process. The nitrogen plasma treatment converts the top several nanometres of the surface to silicon oxynitride phases[21], and these decompose readily during the CVD process at greater temperature and act as an additional source of bubbles under the graphene. After the plasma nitridation of the substrate, Cu catalyst is sputtered onto the surface and growth of graphene is performed by ICP-CVD. The graphene/Cu/SiO_2/Si wafer is then coated with polymethyl methacrylate (PMMA) for protection and immersed in an aqueous etchant bath. The Cu film is then etched (Supplementary Figs 3 and 4). Throughout, the PMMA/graphene film adheres firmly to the underlying wafer. It is worth pointing out that our face-to-face transfer process has a shorter Cu etching time than does conventional float transfer (Fig. 2a). The Cu film can usually be completely dissolved within 2 h, even in dilute etchant.

To estimate the thickness of the infiltrated water layer, we produced an 8-inch SiO_2/Si wafer onto which a graphene layer had been transferred by our face-to-face process; this wafer, with the layer structure

[1]Graphene Research Centre, National University of Singapore, 6 Science Drive 2, 117546 Singapore. [2]Department of Chemistry, National University of Singapore, 3 Science Drive 3, 117543 Singapore. [3]Department of Physics, National University of Singapore, 2 Science Drive 3, 117542 Singapore.

©2014 Macmillan Publishers Limited. All rights reserved

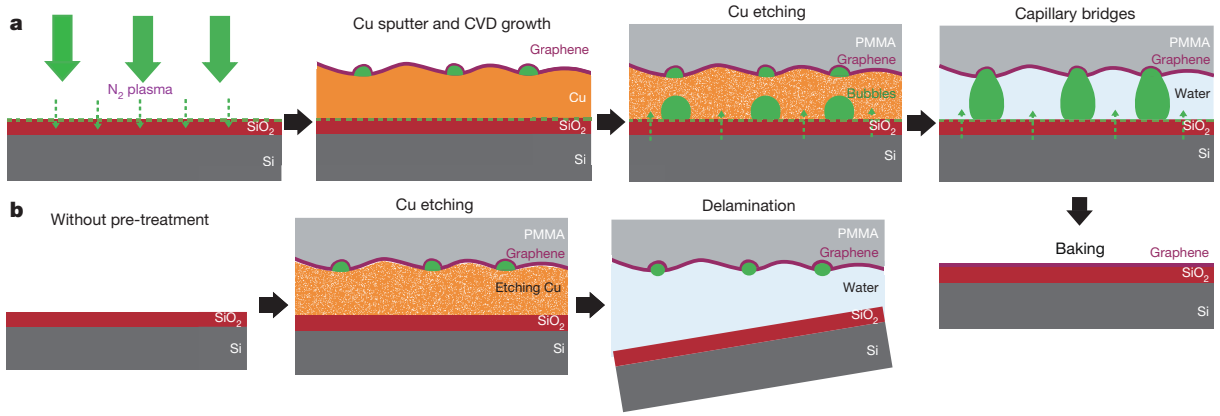


Figure 1 | Illustration of our face-to-face method for transferring graphene mediated by capillary bridges. **a**, Schematic illustration showing 'bubble seeding' by plasma treatment, CVD growth, Cu film etching, formation of capillary bridges and removal of water and PMMA. See text for details. **b**, Schematic illustration showing that in the absence of plasma treatment, delamination of the film results.

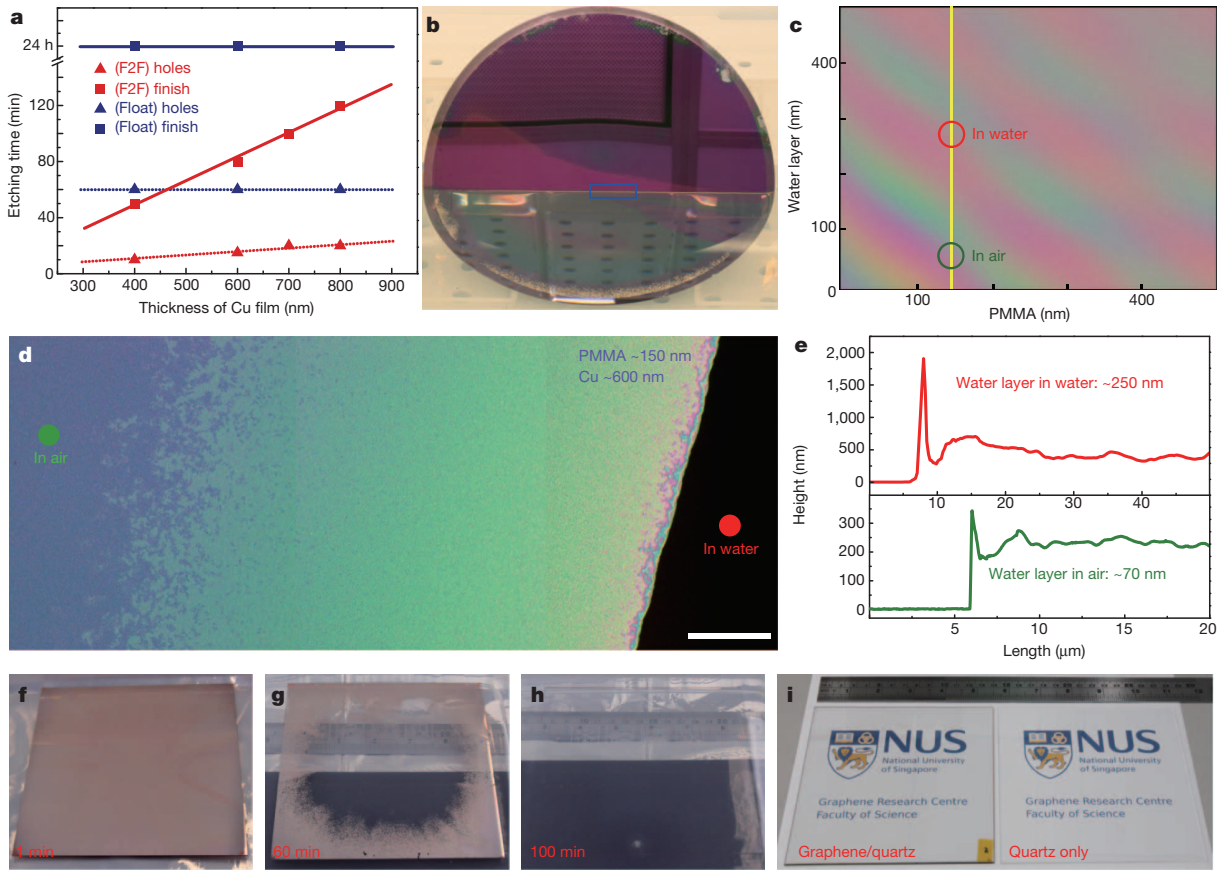


Figure 2 | Characterization of intercalated water layer with capillary bridges during face-to-face transfer. **a**, Comparison of etching time between face-to-face (F2F) and float transfer. The triangles indicate the time when visible holes in the copper film appear, and the squares indicate the time of complete etching of the Cu film. **b**, Photograph of a partially submerged 8-inch PMMA/graphene/water layer/SiO_2/Si wafer in water. The blue box shows the border between water/PMMA/water and air/PMMA/water interfaces. **c**, Simulated colour change of the PMMA/graphene/water layer/SiO_2/Si wafer placed in air. Red and green circles indicate sampling positions for data in **e**. The vertical yellow line indicates the relevant data for different thicknesses of the water layer and a fixed thickness of 150 nm for the PMMA layer, which is used here. **d**, Optical image of PMMA/graphene at the water–air border. The red dot identifies the bulk water. Scale bar, 500 μm. **e**, AFM profiles of thicknesses of PMMA/graphene with infiltrated water layer, measured in water (top) and in air (bottom). **f**–**h**, Photographs of PMMA/graphene/Cu (700 nm)/quartz (14 cm) immersed in Cu etchant for different times (given in red at bottom of panels), showing that the face-to-face transfer also works on quartz. **i**, Left, photograph of face-to-face transferred graphene on quartz after removal of PMMA and baking. Right, quartz only.

©2014 Macmillan Publishers Limited. All rights reserved

PMMA/graphene/water layer/SiO_2/Si, was pulled out partially from water for optical characterization (Fig. 2b). The combined effects of reflection and refraction of light at the multiple interfaces can be simulated using the CIE (International Commission on Illumination) colour-matching equation to reproduce the colour change[22,23] (Fig. 2c; the method is illustrated in Supplementary Fig. 5). The observed colour change of the PMMA/graphene/water layer/SiO_2/Si system is due to the change in thickness of the water layer under the graphene as it escapes, which generates coloured fringes (Fig. 2d). The PMMA/graphene floating on infiltrated water at the air–water border is pale red in colour (right) at first, and changes into olive, green and violet as the thickness of water layer decreases. On the basis of the simulated colour changes, the thickness of the intercalated water layer is estimated to be 60–80 nm in air (violet) and 250–300 nm in water (pale red). To confirm this measurement, the thickness of intercalated water layer when the wafer is immersed in water is determined by an AFM that can perform measurements under water, and its thickness in air after some water escapes is measured by a fast-scan AFM (Supplementary Fig. 6). Figure 2e shows that the mean thickness of the water layer when the wafer is under water has a mean value of ~250 nm, and that the thickness in air is ~70 nm. These values agree with the simulation in Fig. 2c, marked by circles. It is worth noting that the change in height profile is reversible when the wafer is immersed into water or withdrawn from it again; this implies that water can infiltrate freely in the intercalated layer between graphene and the substrate. The infiltrated water can be completely evaporated by baking the wafer at 150 °C for more than 10 min, producing a dry graphene film on SiO_2/Si. The face-to-face transfer also works on quartz substrates, as shown in Fig. 2f–i for a 700-nm sputtered Cu film on a 14 cm × 14 cm quartz plate.

The Greenwood–Williamson contact mechanics theory adapted to randomly rough surfaces in close contact can be used to estimate the maximal height of the capillary bridges formed at the interface[24,25]. PMMA/graphene can be considered an elastic soft surface in contact with a hard and rough substrate (Cu/SiO_2/Si). In the contact region between the two surfaces, a liquid capillary bridge will form. The meniscus radius r_K is given by the Kelvin equation, $r_K = -\gamma v_0/(k_B T)\ln(P_v/P_{sat})$, where γ is the surface tension, P_v is the actual vapour pressure, P_{sat} is the saturated vapour pressure, v_0 is the molar volume of water, k_B is Boltzmann's constant and T is temperature, and the thickness of the water is given by $d_K = r_K(\cos\theta_1 + \cos\theta_2)$, where θ_1 and θ_2 are the contact angles of the two surfaces[25].

When the PMMA/graphene is almost delaminating from the wafer surface because of a pull-off force, d_K becomes largest. At this point, the work of adhesion (w; equation (1)) will be decreased to zero, and the maximal height of the capillary bridge (d_c) can be estimated from equation (2)[25]:

$$w \approx 2\gamma\left[1 - \frac{h}{2d_K}\ln\left(\frac{q_0 h E d_K}{2\gamma}\right)\right] \quad (1)$$

$$d_c = \frac{h}{2}\ln\left(\frac{q_0 h E d_c}{2\gamma}\right) \quad (2)$$

Here q_0 is the roll-off wavevector of the surface roughness power spectrum, h is the roughness and E is the Young's modulus of the film. Accordingly, d_c is calculated to be in the range 300–450 nm by assuming a roughness of h = 100–150 nm for the PMMA/graphene (root mean squared roughness as determined by AFM). The significance of d_c is that it sets an upper limit on the thickness of the Cu films that can be sputtered onto the SiO_2/Si surface, because a thick Cu film will result in the infiltration of a thick water layer that exceeds the threshold thickness d_c. As observed in our experiments, if the thickness of the Cu film is three times larger than d_c, then delamination of the PMMA/graphene film occurs as a result of the infiltration of an excessively thick water layer. Under typical conditions, the thickness of the infiltrated water is about one-third the thickness of the Cu film because hydrostatic pressure compresses the film after the removal of the Cu. Owing to the fact that PMMA/graphene is a soft membrane, it can deform elastically in response to the capillary forces caused by the gas bridges, and this allows the film to be pulled closer to the hard substrate.

The high surface tension of water exerts a pulling force on the graphene, and undesirable ripples and folds are created. The surface tension can be reduced by adding isopropyl alcohol or by increasing the temperature of the water (to 80 °C). Figure 3a is a typical AFM image of a face-to-face graphene film on a SiO_2/Si wafer, where a high density of graphene nanobubbles with heights up to ~20 nm can be seen. After the addition of isopropyl alcohol (Fig. 3b) or increasing water temperature (Fig. 3c), there is a significant reduction in the density of graphene wrinkles, and the height of the nanobubbles is reduced by a factor of at least ten, resulting in a visible flattening of the film. Therefore, the addition of a surfactant into the water can help to 'iron out' the creases on the graphene during the face-to-face transfer process.

Figure 4a shows a photograph of face-to-face transferred graphene on SiO_2/Si wafers after removing PMMA (both a 4-inch and an 8-inch wafer are shown). The transferred graphene film appears to be highly uniform, with no visible transfer defects such as cracks and folds, and its torn edges can be observed by the naked eye (Fig. 4a inset). Raman spectroscopy is a commonly applied technique for characterizing the properties of graphene in terms of its layer number, defects and doping[26,27]. The Raman spectra of graphene transferred by face-to-face and, respectively, conventional float transfer are shown in Fig. 4b, displayed together with the spectrum of graphene on a Cu film as a reference. Although as-grown graphene before transfer shows nearly no defect-related D band (at ~1,350 cm^{-1}), both face-to-face and float-transferred graphene show small D peaks due to the Raman signal enhancement on a dielectric substrate[28]. The 2D band (at ~2,690 cm^{-1}), which is due to two phonons with opposite momenta in the highest optical branch, is

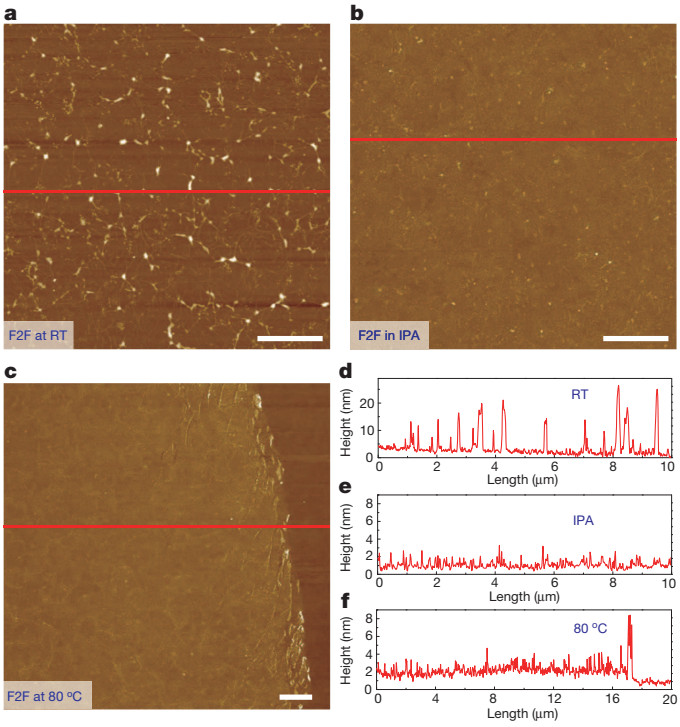


Figure 3 | AFM images and height profiles of graphene on a SiO_2/Si wafer transferred by our face-to-face technique. **a–c**, AFM images of films transferred in room-temperature (RT) water (**a**); in room-temperature isopropyl alcohol (IPA; **b**); and in water at 80 °C (**c**). **d–f**, Corresponding height profiles for **a–c**, respectively. The red horizontal line in **a–c** shows the related profile positions for **d–f.** The density of the nanobubbles decreases after reducing the liquid surface tension in **b** and **c**. Scale bars, 2 μm.

©2014 Macmillan Publishers Limited. All rights reserved

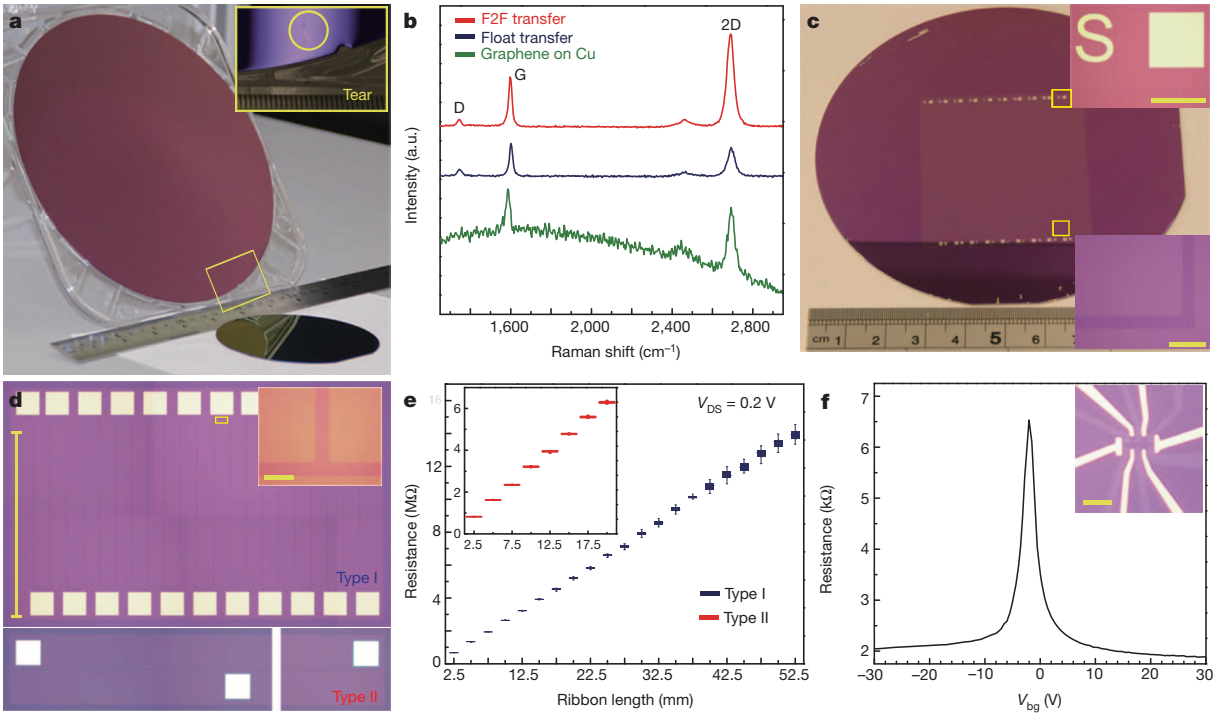


Figure 4 | Characterization of face-to-face transferred graphene on a SiO_2/Si wafer. **a**, Photograph of face-to-face transferred graphene on an 8-inch wafer and a 4-inch wafer; the boxed area is shown enlarged in the inset, where a torn edge shows the presence of a graphene sheet. **b**, Raman spectra of graphene prepared by face-to-face transfer (red) and by float transfer onto SiO_2/Si substrates (blue), and of graphene on Cu film before transfer (green). a.u., arbitrary units. **c**, Photograph of unbroken 1-m-long and 15-μm-wide zigzag graphene ribbon on face-to-face transferred graphene wafer. Insets at top and bottom right are magnified optical images from the positions marked by yellow boxes. 'S' is a location marker for the metal electrode on the ribbons. **d**, Optical image of a graphene ribbon 5 cm long and 10 μm wide. The graphene ribbon is fabricated in a zigzag configuration (top panel, type I) and as a straight ribbon (bottom panel, type II); inset at top right is the zoomed optical image for type I, from the position marked by the yellow box. **e**, Box plot showing resistance versus length for graphene ribbons of type I and type II. The linear relationship between resistance and length shows the long-distance continuity of the ribbons. All the measurements were performed at a voltage (V_{DS}) of 0.2 V between two electrodes. **f**, Carrier mobility for a monolayer graphene Hall bar device under ambient conditions; the Hall effect mobility of this device is ~3,800 $cm^2 V^{-1} s^{-1}$. Inset, optical image of the related graphene Hall bar device. V_{bg} is the gate voltage during the measurement. Scale bars: **d** (main panel), 2.5 mm; in insets of **c**, **d** and **f**, 1 mm (top right), 20 μm (bottom right), 20 μm and 5 μm, respectively.

more sensitive to long-range order. Here it can be seen that the intensity of the 2D band is much higher in face-to-face than float-transferred graphene, which attests to the higher crystalline quality of the former. More characterization of the as-grown graphene is shown in Supplementary Figs 8 and 9. X-ray photoelectron spectroscopy is used to check the phase purity of face-to-face transferred graphene film on a SiO_2/Si wafer (Supplementary Fig. 11). There is no detectable Cu on the surface within the sensitivity of the technique. Residual N can be detected on the wafer (at 398 eV) but this is distinct from N dopants in graphene[29] and is attributed to implanted N species in the silicon oxynitride phase[21].

The electrical properties of face-to-face transferred graphene films are investigated by standard micro/nanofabrication processes. To test the robustness of this transfer process with regard to crack-free and continuous films, long graphene ribbons were fabricated (up to 1 m long and 15 μm wide in Fig. 4c; 5 cm long and 10 μm wide in Fig. 4d; details in Supplementary Information). The resistivity is measured by a standard four-probe station after applying a 50 nm Ni layer as metal electrodes. As shown in Fig. 4e, the measured resistances exhibit linearity with the length of the ribbon, and a conductivity of ~4,000 S cm^{-1} can be achieved, thus attesting to the long-distance continuity of the film after transfer. To the best of our knowledge, continuous, uninterrupted graphene ribbons with length/width ratios of more than 10^5 are seldom demonstrated, because cracks are inevitable in the wet or dry transfer processes; thus, the face-to-face transfer method developed here is unique in enabling high-fidelity, crack-free transfer. To evaluate the electronic quality of the face-to-face transferred graphene grown by ICP-CVD at 750 °C, standard electron-beam lithography is used to fabricate graphene Hall bars on a Si wafer with a 290-nm SiO_2 layer. A typical optical image of these graphene Hall bars is shown Fig. 4f, inset. Four metal electrodes of Cr/Au (5/50 nm) are used to eliminate the contact resistance, and the transport characteristics of the device are measured under ambient conditions. The transport result for this device is shown in Fig. 4f, and the extracted carrier mobilities of electrons and holes for this device are both ~3,800 $cm^2 V^{-1} s^{-1}$, which is comparable to the properties of thermal CVD graphene grown at much higher temperature[4,6,17,30]. The slightly negative Dirac point indicates that the transferred graphene is weakly n-type doped[17].

All the characterization above shows that the face-to-face transferred films maintain good crystalline integrity and long-distance continuity without cracks. The copper catalyst can be effectively removed and the carrier mobility of the film is comparable to that of thermal CVD-grown film prepared at higher temperatures. The key advantages of this face-to-face transfer are that it is relatively easy and requires only a simple pretreatment step followed by immersion in a suitable etchant; it resembles a spontaneous transfer process because there is no recovery of floating graphene needed; and, most importantly, the non-manual and wafer-compatible nature of the method suggests that it is automation-compatible and industrially scalable. Interestingly, we have found that water has the ability to infiltrate between the graphene and the wafer substrate, thus allowing the addition of different surfactants for modifying the interfacial tension and reducing the corrugations in graphene film. Although there are many potential applications of the roll-to-roll transfer method[6] owing to its applicability to flexible devices, it must be noted that so far most devices operate on 'stiff' substrates such as silicon, and that a non-manual, batch-processed transfer method serving this technology segment is definitely needed. The face-to-face transfer

©2014 Macmillan Publishers Limited. All rights reserved

method will be very useful as an enabler for rapidly emerging graphene-on-silicon platforms that have shown excellent promise for devices such as a gate-controlled Schottky barrier triode device[8] and an optical modulator[9]. Finally, the face-to-face transfer method should be applicable to all CVD growth on a metal-catalyst-coated wafer, such as hexagonal BN and transition-metal chalcogenide films.

METHODS SUMMARY

The catalyst preparation and ICP-CVD growth are both performed in a customized sputter/electron-beam/ICP-CVD cluster. First, 8-inch or 4-inch SiO_2/Si (or quartz) wafers are sputtered with Cu films at 100–200 °C. For face-to-face transfer, the wafers are pre-treated with N_2 plasma (1,000 W, 50 mtorr). The conditions for ICP-CVD growth are as follows: the wafer with a sputtered Cu film is treated with a H_2 plasma (150 W) for 5 min with the substrate heated to 750 °C at 50 mtorr. A mixture of H_2 and CH_4 (H_2:CH_4 = 150:10) is introduced into the chamber for graphene growth (150 W plasma power, 50 mtorr, 5 min). After growth, the graphene/Cu/wafer is spin-coated with PMMA (996,000 relative molecular mass, 4 wt% in ethyl lactate, 3,000 r.p.m. for 1 min) for protection. A 0.1 M ammonium persulphate ($(NH_4)_2S_2O_8$) aqueous solution or 1 M iron chloride ($FeCl_3$) is used as the etchant. Baking at 150 °C for 10 min is needed to evaporate the water layer. Finally, face-to-face transferred graphene on the wafer is realized by removing the PMMA with acetone.

Raman spectra of graphene films are collected using a 532-nm laser under ambient conditions (WITec alpha 300 R). The AFM measurements were performed in tapping mode (Bruker Dimension FastScan), and a liquid AFM was used to measure the thickness of PMMA/graphene in water (Agilent 5420). All coloured optical images are captured with a Nikon Eclipse LV100D. Long graphene ribbons are fabricated by a laser writer (MicroTech LW405B), and graphene Hall bars are patterned by electron beam lithography (Nova NanoSEM 230). Electron-beam-evaporated 50-nm Ni films are used as contacts for the long ribbons, and thermally evaporated 5-nm Cr and 50-nm Au films are used as metal contacts for the Hall bars. Current–voltage curves are measured by a four-probe station under ambient conditions (Keithley 4200 SCS and 6430).

Online Content Any additional Methods, Extended Data display items and Source Data are available in the online version of the paper; references unique to these sections appear only in the online paper.

Received 8 July; accepted 10 October 2013.
Published online 11 December 2013.

1. Novoselov, K. S. *et al.* Electric field effect in atomically thin carbon films. *Science* **306,** 666–669 (2004).
2. Novoselov, K. S. *et al.* Two-dimensional atomic crystals. *Proc. Natl Acad. Sci. USA* **102,** 10451–10453 (2005).
3. Novoselov, K. S. *et al.* A roadmap for graphene. *Nature* **490,** 192–200 (2012).
4. Li, X. S. *et al.* Large-area synthesis of high-quality and uniform graphene films on copper foils. *Science* **324,** 1312–1314 (2009).
5. Gao, L. B. *et al.* Efficient growth of high-quality graphene films on Cu foils by ambient pressure chemical vapor deposition. *Appl. Phys. Lett.* **97,** 183109 (2010).
6. Bae, S. K. *et al.* Roll-to-roll production of 30-inch graphene films for transparent electrodes. *Nature Nanotechnol.* **5,** 574–578 (2010).
7. Kang, J. *et al.* Efficient transfer of large-area graphene films onto rigid substrates by hot pressing. *ACS Nano* **6,** 5360–5365 (2012).
8. Yang, H. *et al.* Graphene barristor, a triode device with a gate-controlled Schottky barrier. *Science* **336,** 1140–1143 (2012).
9. Liu, M. *et al.* A graphene-based broadband optical modulator. *Nature* **474,** 64–67 (2011).
10. Chen, J. Y. *et al.* Oxygen-aided synthesis of polycrystalline graphene on silicon dioxide substrates. *J. Am. Chem. Soc.* **133,** 17548–17551 (2011).
11. Federle, W., Barnes, W. J. P., Baumgartner, W., Drechsler, P. & Smith, J. M. Wet but not slippery: boundary friction in tree frog adhesive toe pads. *J. R. Soc. Interface* **3,** 689–697 (2006).
12. Persson, B. N. J. Wet adhesion with application to tree frog adhesive toe pads and tires. *J. Phys. Condens. Matter* **19,** 376110 (2007).
13. Reina, A. *et al.* Large area, few-layer graphene films on arbitrary substrates by chemical vapor deposition. *Nano Lett.* **9,** 30–35 (2009).
14. Kim, K. S. *et al.* Large-scale pattern growth of graphene films for stretchable transparent electrodes. *Nature* **457,** 706–710 (2009).
15. Gao, L. B. *et al.* Repeated growth and bubbling transfer of graphene with millimetre-size single-crystal grains using platinum. *Nature Commun.* **3,** 699 (2012).
16. Li, X. S. *et al.* Large-area graphene single crystals grown by low-pressure chemical vapor deposition of methane on copper. *J. Am. Chem. Soc.* **133,** 2816–2819 (2011).
17. Sun, Z. Z. *et al.* Growth of graphene from solid carbon sources. *Nature* **468,** 549–552 (2010).
18. Levendorf, M. P. *et al.* Graphene and boron nitride lateral heterostructures for atomically thin circuitry. *Nature* **488,** 627–632 (2012).
19. Rafiee, J. *et al.* Wetting transparency of graphene. *Nature Mater.* **11,** 217–222 (2012).
20. Bunch, J. S. *et al.* Impermeable atomic membranes from graphene sheets. *Nano Lett.* **8,** 2458–2462 (2008).
21. Kobayashi, H., Mizokuro, T., Nakato, Y., Yoneda, K. & Todokoro, Y. Nitridation of silicon oxide layers by nitrogen plasma generated by low energy electron impact. *Appl. Phys. Lett.* **71,** 1978–1980 (1997).
22. Gao, L. B., Ren, W. C., Li, F. & Cheng, H. M. Total color difference for rapid and accurate identification of graphene. *ACS Nano* **2,** 1625–1633 (2008).
23. Janos, S. *Colorimetry: Understanding the CIE System* 25–88 (Wiley, 2007).
24. Greenwood, J. A. & Williamson, J. B. P. Contact of nominally flat surfaces. *Proc. R. Soc. Lond. A* **295,** 300–319 (1966).
25. Persson, B. N. J. Capillary adhesion between elastic solids with randomly rough surfaces. *J. Phys. Condens. Matter* **20,** 315007 (2008).
26. Ferrari, A. C. *et al.* Raman spectrum of graphene and graphene layers. *Phys. Rev. Lett.* **97,** 187401 (2006).
27. Das, A. *et al.* Monitoring dopants by Raman scattering in an electrochemically top-gated graphene transistor. *Nature Nanotechnol.* **3,** 210–215 (2008).
28. Gao, L. B. *et al.* Surface and interference coenhanced Raman scattering of graphene. *ACS Nano* **3,** 933–939 (2009).
29. Wei, D. C. *et al.* Synthesis of N-doped graphene by chemical vapor deposition and its electrical properties. *Nano Lett.* **9,** 1752–1758 (2009).
30. Yoon, T. *et al.* Direct measurement of adhesion energy of monolayer graphene as-grown on copper and its application to renewable transfer process. *Nano Lett.* **12,** 1448–1452 (2012).

Supplementary Information is available in the online version of the paper.

Acknowledgements We thank C. T. Nai for help with X-ray photoelectron spectroscopy and B. K. Chong (Agilent Technologies) for the liquid AFM. This work was supported by MOE Tier 2 grant 'Interface engineering of graphene hybrids for energy conversion' (R-143-000-488-112) and by NRF-CRP grant 'Novel 2D materials with tailored properties: beyond graphene' (R-144-000-295-281).

Author Contributions L.G. and K.P.L. designed the experiments, interpreted the data and wrote the manuscript. L.G. performed graphene growth, transfer and calculations. L.G., G.-X.N. and B.L. fabricated the devices. Y.L. performed the X-ray photoelectron spectroscopy measurements. L.G., K.P.L. and A.H.C.N. discussed the data.

Author Information Reprints and permissions information is available at www.nature.com/reprints. The authors declare no competing financial interests. Readers are welcome to comment on the online version of the paper. Correspondence and requests for materials should be addressed to K.P.L. (chmlohkp@nus.edu.sg).

©2014 Macmillan Publishers Limited. All rights reserved